SOILS AND FOUNDATIONS Vol. 45, No. 4, 13–25, Aug. 2005
Japanese Geotechnical Society

A RECONSIDERATION OF THE SAFETY OF PILED BRIDGE FOUNDATIONS IN LIQUEFIABLE SOILS

S. BHATTACHARYA[i], M. D. BOLTON[ii] and S. P. G. MADABHUSHI[iii]

ABSTRACT

The collapse of piled foundations in liquefiable soil has been observed in the majority of recent strong earthquakes. This paper critically reviews the current understanding of pile failure in liquefiable deposits, making reference to modern design codes such as JRA (1996), and taking the well-documented failure of the Showa Bridge in the 1964 Niigata earthquake as an example of what must be avoided. It is shown that the current understanding cannot explain some observations of pile failure. The current method of pile design under earthquake loading is based on a lateral loading mechanism where inertia and drag due to slope movement (lateral spreading) induce bending in the pile, and where axial load effects are ignored. It is demonstrated here, however, that axial loads can be a dominant factor in collapse due to seismic liquefaction, due to the progressive onset of pile buckling when lateral soil resistance is removed. Additional design considerations based on the avoidance of buckling effects are formulated after back analysing fifteen case histories of pile foundation performance during past earthquakes, and verified using dynamic centrifuge modelling. Some practical implications of the omission of axial loads from previous design verifications are highlighted.

Key words: buckling, case histories, centrifuge tests, earthquakes, failure, lateral spreading, liquefaction, piles, Showa Bridge (**IGC**: E4/E8/E12)

INTRODUCTION

Structural failure of piles passing through liquefiable soils has been observed in many of the recent strong earthquakes. This suggests that the bending moments or shear forces that are experienced by the piles exceed those predicted by their design methods (or codes of practice). The Japanese Road Association Code (JRA, 1996) does consider the effects of soil liquefaction, which it assumes are related to the drag on the piles caused by lateral spreading of the soil, as in National Research Council (NRC, 1985), Hamada (1992a, 1992b, 2000), Ishihara (1993, 1997), Finn and Thavaraj (2001), Finn and Fujita (2002), Abdoun and Dobry (2002). All current design codes apparently provide a high margin of safety using conservatively high characteristic loads and apparently substantial partial safety factors on material resistances, yet occurrences of pile failure due to liquefaction are abundant. This implies that the actual moments or shear forces experienced by such piles are many times higher than the predictions. It must be concluded that the current design methods may not be consistent with the physical processes or mechanisms that govern liquefaction-induced failure. This paper investigates buckling as an alternative mechanism for pile failure due to soil liquefaction. Reference is made to the well-known failure of the Showa Bridge and to 15 other field case studies, as well as to centrifuge model tests.

CURRENT UNDERSTANDING OF LIQUEFACTION-INDUCED PILE FAILURE

The current understanding of pile failure as expressed in the literature and design codes is as follows. Soil liquefies, losing its shear strength, causing it to flow taking with it any overlying non-liquefied crust. These soil layers drag the pile with them, causing a bending failure. This is often referred to as failure due to lateral spreading. In terms of soil-pile interaction, the current mechanism of failure assumes that the soil pushes the pile. The Japanese Highway code of practice (JRA, 1996) has incorporated this concept as shown in Fig. 1. The code advises practising engineers to design piles against bending failure assuming that the non-liquefied crust exerts passive earth pressure on the pile and the liquefied soil offers 30% of total overburden pressure. Yokoyama et al. (1997) reports that this code was formulated by back analysing a few piled bridge foundations of the

[i] STAFF Engineer, Fugro Limited, U.K. (S.Bhattacharya.00@cantab.net, sbhattacharya@fugro.co.uk) (formerly 21st Century Centre of Excellence Fellow, Centre for Urban Earthquake Engineering, Tokyo Institute of Technology, Japan).
[ii] Professor of Soil Mechanics, Department of Engineering, Cambridge University, U.K. (mdb@eng.cam.ac.uk).
[iii] Senior Lecturer, ditto (mspg1@eng.cam.ac.uk).
The manuscript for this paper was received for review on October 6, 2003; approved on May 30, 2005.
Written discussions on this paper should be submitted before March 1, 2006 to the Japanese Geotechnical Society, 4-38-2, Sengoku, Bunkyo-ku, Tokyo 112-0011, Japan. Upon request the closing date may be extended one month.

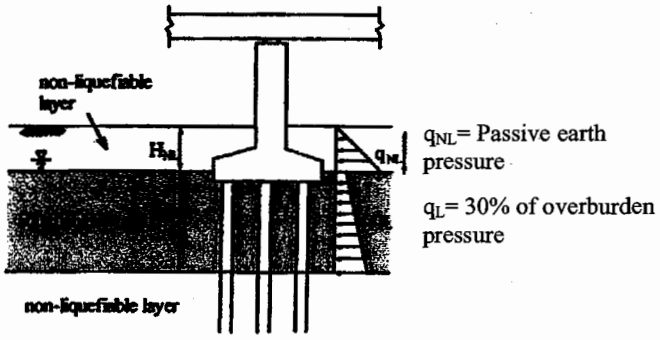

Fig. 1. JRA (1996) code of practice showing the idealisation for seismic design of bridge foundation

Hanshin expressway that were not seriously damaged following the 1995 Kobe earthquake.

Inertia of the superstructure can also induce bending moments in the pile. However, Ishihara (1997) notes that, the onset of liquefaction takes place approximately at the instant of peak acceleration during the course of seismic load application with an irregular time history. He argues that since the seismic motion has already passed its peak, such shaking as may persist will be less intense, so that the inertia force transmitted to the superstructure will not be significant. Hamada (2000) in the 12th World Congress on Earthquake Engineering concluded that permanent displacement of non-liquefied soil overlying the liquefied soil is a governing factor for pile damage. A similar conclusion has also been reached by Berrill et al. (2001).

Codes of practice such as JRA (1996), the USA code (NEHRP, 2000), Eurocode 8, part 5 (1998) and the Indian code (IS, 1893, 2002) focus their demand for calculations on the bending strength of the pile in relation to bending moments induced by lateral spreading. Work studying this pile failure mechanism has been conducted by various researchers, such as Takahashi et al. (2002), Tokimatsu et al. (2001), Berrill et al. (2001), and Ramos et al. (2000). Sato et al. (2001) used stress cell measurements to conclude that the forces predicted by JRA (1996), and illustrated in Fig. 1, are over-conservative. The centrifuge test results of Haigh and Madabhushi (2002) suggest that the pressure distribution in Fig. 1 is under-conservative in the transient phase but gives reasonable predictions for residual sliding.

Of course, codes of practice have to specify some simple design loads (including earth pressures, in this case) which should provide a safe working envelope for any structure of the class being considered, and in the full range of ground conditions likely to be encountered at different sites. The degree of accuracy in any one given case is not the most important facet of a rule such as that shown in Fig. 1. Our concern in this paper is not to criticise provisions such as those in Fig. 1, but to point out that the application of any such lateral loading condition demands further consideration of the effective lateral stiffness of the pile taking axial load into account. Crucially, this requires that the pile must not be close to buckling when the surrounding soil liquefies.

PILE BUCKLING

Structural engineers would have to regard piles as slender columns were it not for the lateral support they receive from the surrounding soil. Generally, as the length of a pile increases, the allowable axial load on the pile also increases, due to additional shaft friction and also to the enhanced base capacity that comes from stronger strata. However, the elastic buckling load (if an end-bearing pile were laterally unsupported by soil) decreases inversely with the square of its length following Euler's formula. Figure 2 shows a typical variation with depth of Euler's elastic critical load (P_E) for a pile that receives no lateral bracing from surrounding soil. The pile in this example has an external diameter of 609 mm and a wall thickness of 9 mm and is passing through liquefiable soil. The elastic critical load (P_E) is a conventional static estimate, based on the removal of soil lateral stiffness due to soil liquefaction, the pile being fixed into a rock-socket at the base but free to rotate at the top. Also shown is the plastic squash load (P_P) that would separately apply if the pile section were compressed in the absence of bending and buckling; a plastic yield stress of 500 MPa was adopted.

Rankine (1866) recognised that the actual failure of structural columns involved an interaction between elastic and plastic modes of failure. Lateral loads, or geometrical imperfections, lead to the creation of bending moments in addition to axial loads. Bending moments have to be accompanied by stress resultants that diminish the cross-sectional area available for carrying the axial load, so the failure load $P_F < P_P$. Equally, the growth of zones of plastic bending reduces the effective elastic modulus of the section, thereby reducing the critical load for buckling, so that $P_F < P_E$. Furthermore these processes feed on each other, as explained in Horne and Merchant (1965). As the elastic critical load is approached, all bending effects are magnified. If lateral loads in the absence of axial load would create a maximum lateral displacement δ_o in the critical mode-shape of buckling, then the displacement δ under the same lateral loads but with a co-existing axial load P is given by:

$$\delta/\delta_o = 1/(1 - P/P_E) \quad (1)$$

The same magnification factor applies to any initial out-of-straightness of the pile in the mode-shape of potential buckling. Correspondingly, all curvatures are similarly magnified and so are the bending strains induced in the column by its lateral loads or eccentricities. The progression towards plastic bending failure is accelerated as axial loads approach the elastic critical load. Not only do axial loads induce extra bending moments (P-δ effects), but the full plastic bending resistance can not be mobilised due to that part of the section required to carry the axial loads. An interaction formula to estimate the actual failure load P_R in plastic buckling, following Rankine's suggestion, and supported by subsequent research on the collapse of building frames, was recommended by Horne and Merchant.

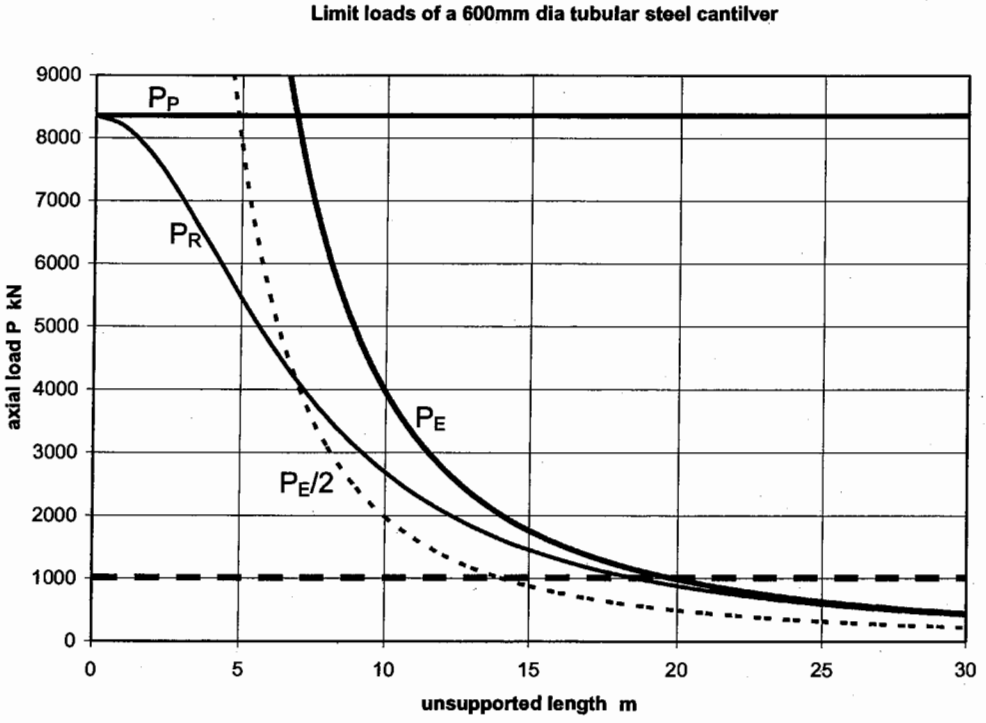

Fig. 2. Limiting axial loads for an unsupported tubular steel cantilever—plastic squash load P_P, Euler's elastic buckling load P_E, Rankine's elastic-plastic buckling load P_R

(1965):

$$1/P_R = 1/P_E + 1/P_P \quad (2)$$

and this is also plotted in Fig. 2. Structural engineers apply one or other interaction formula of this type to columns, i.e. to members in a building frame whose main purpose is the transmission of axial load. Its application to foundation piles is therefore equally essential so long as it is accepted that soil liquefaction removes all effective lateral bracing.

Evidently, the cantilever pile described in Fig. 2 would be expected by Rankine's formula to fail by plastic buckling under an axial load of 1000 kN, for example, if its unsupported length exceeded about 18 m. However, structural engineers invariably demand a high factor of safety against linear elastic buckling to allow for the additional effects of lateral loading. Equation (1) indicates that for a column carrying an axial load of half its Euler load, that lateral displacements and bending moments would be $1/(1-1/2)$ or 100% bigger than those calculated ignoring axial load effects. This is clearly important if significant lateral forces must also be carried. It should therefore be considered essential to place the design point in Fig. 2 well below the $P_E/2$ line, which lies below Rankine's failure load P_R for long columns under axial load alone. If the tubular pile of Fig. 2 were used to support an axial load of 1000 kN over an unsupported length of 14 m, and under the influence of significant lateral loads, it would be likely to collapse.

Piles are likely to have greater out-of-straightness, more significant yielding during construction, more deterioration during life, and more uncertainty in their lateral loading during earthquakes, than is the case with ordinary structural columns in buildings. Furthermore, the consequences of plastic buckling failure is invariably catastrophic. The creation of a full plastic mechanism due to the amplification of lateral load effects would lead immediately to the Euler buckling load reducing to zero, so that the superstructure must collapse suddenly and violently unless its self-weight can immediately be transferred to foundation elements that can still carry load. It would therefore be unwise to use a factor of safety less than 3 against the Euler load of a pile. Correspondingly, the 0.6 m diameter pile analysed in Fig. 2 should not be designed to carry 1000 kN over an unsupported length in excess of about 11 m. The question remains whether earthquake-induced liquefaction can actually eliminate sufficient lateral soil stiffness, for a long enough period of time, to promote pile buckling in the manner set out above—this is now explored.

STUDY OF CASE HISTORIES

In this study, fifteen reported cases of pile foundation performance during earthquake-induced liquefaction have been studied and analysed as listed in Table 1. Six of the piled foundations were found to survive while the others suffered severe damage (Bhattacharya et al., 2004). The parameters r_{min} (minimum radius of gyration) and L_{eff} (effective buckling length of the pile) are introduced to analyse the piles, as follows.

1. r_{min}: The minimum radius of gyration of the pile section about any axis of bending (m). This parameter can represent piles of any shape (square, tubular or solid

Table 1. Summary of case histories, Bhattacharya et al. (2004)

ID in Fig. 4	Case history and reference	Pile section/type	L_0* (m)	L_{eff} (m)	r_{min} (m)
A	10 storey-Hokuriku Building, Hamada (1992a)	0.4 m dia RCC	5	5	0.1
B	Landing Bridge, Berrill et al. (2001)	0.4 m square PSC	4	2	0.12
C	14 storey Building, Tokimatsu et al. (1996)	2.5 m dia RCC	12.2	12.2	0.63
D	Hanshin Expressway Pier, Ishihara (1997)	1.5 m dia RCC	15	15	0.38
E	LPG Tank 101, Ishihara (1997)	1.1 m dia RCC	15	15	0.28
F	Kobe Shimim Hospital, Soga (1997)	0.66 m dia steel tube	6.2	6.2	0.23
G	N.H.K Building, Hamada (1992a)	0.35 m dia RCC	10	20	0.09
H	NFCH Building, Hamada (1992a)	0.35 m dia RCC hollow	8	16	0.10
I	Yachiyo Bridge Hamada (1992a)	0.3 m dia RCC	8	16	0.08
J	Gaiko Warehouse, Hamada (1992b)	0.6 m dia PSC hollow	14	28	0.16
K	4 storey Firehouse, Tokimatsu et al. (1996)	0.4 m dia PSC	18	18	0.10
L	3 storied Building at Kobe University, Tokimatsu et al. (1998)	0.4 m dia PSC	16	16	0.12
M	Elevated Port Liner Railway, Soga (1997)	0.6 m dia RCC	12	12	0.15
N	LPG Tank -106,107, Ishihara (1997)	0.3 m dia RCC hollow	15	15	0.08
O	Showa Bridge, Hamada (1992a)	0.6 m dia steel tube	19	38	0.21

L_0* = Length of pile in liquefiable layer/buckling zone, *see* Fig. 3(a).

circular) and is used by structural engineers for studying buckling instability. It is given by:

$$r_{min} = \sqrt{\frac{I}{A}} \tag{3}$$

where:

I = second moment area of the pile section about the weakest axis (m^4).

A = area of the pile section (m^2).

For solid circular piles r_{min} is 0.25 times the diameter of the pile and for tubular piles r_{min} is approximately 0.35 times the outside diameter of the pile.

2. L_{eff}: The effective buckling length of the pile, taken from column stability theory. L_{eff} is also familiar as "Euler's buckling length" of a strut pinned at both ends:

$$P_E = \pi^2 EI/L_{eff}^2 \tag{4}$$

Here, it depends on the depth of the unsupported region (L_o) and the boundary fixity conditions of the pile base and pile head as shown in Fig. 3(a). The particular case of a piled raft with piles fixed in direction at the top and bottom of a liquefiable zone, and where $L_{eff} = L_o$, is shown in Fig. 3(b). The assumption of pile fixity calls for significant lateral restraint in the underlying ground, which could be assured only if the piles are grouted into a rock-socket. Fixity at the junction between liquefiable and non-liquefiable soils is, however, impossible. It must be recalled that the base of a liquefied soil layer is at zero effective stress, and therefore acts temporarily as a free surface for any underlying soil. Fixity requires a pile penetration of approximately 5 diameters into dense soil; *see* Fleming et al. (1992). In practice, designers should make a corresponding allowance for imperfect fixity when they select a value for the length L_o that could be left unsupported due to earthquake-induced liquefaction.

The ratio L_{eff}/r_{min} is termed the slenderness ratio of the pile in the region that could become unsupported. Figure 4 plots the L_{eff} against the r_{min} of the pile sections with identification of their performance during earthquakes. A line representing a slenderness ratio (L_{eff}/r_{min}) of 50 is drawn and it distinguishes between unacceptable and acceptable pile performance. This line is of some significance in structural engineering, as it is often used to distinguish between "long" and "short" columns. Columns having slenderness ratios below 50 are expected to fail by plastic squashing whereas those above 50 are expected to fail by buckling, both modes being modified by induced bending moments. Referring back to Fig. 2, a 0.6 m diameter pile fixed at its base and free at the top has $r_{min} = 0.21$ m and $L_{eff} = 2L_o$. A slenderness ratio of 50 therefore translates into a free length $L_o \approx 5$ m for which $P_P < P_E/2$, as expected.

In general, those reporting pile failures have focussed on lateral loading issues, rather than axial load effects. In the cases listed in Table 1, the average pile axial loads P at the time of the earthquake have been estimated rather crudely by assuming them equal to the axial loads that could be considered allowable in conventional designs based on their geometry, and the ground profile at their location. The plot of P and P_E (the elastic buckling load, if unsupported) for the piles that failed in Fig. 4 can be seen in Fig. 5 following Bhattacharya et al. (2004). It may be observed that the piles that failed had a (P/P_E) ratio between 0.5 and 1, and a slenderness ratio (based on the

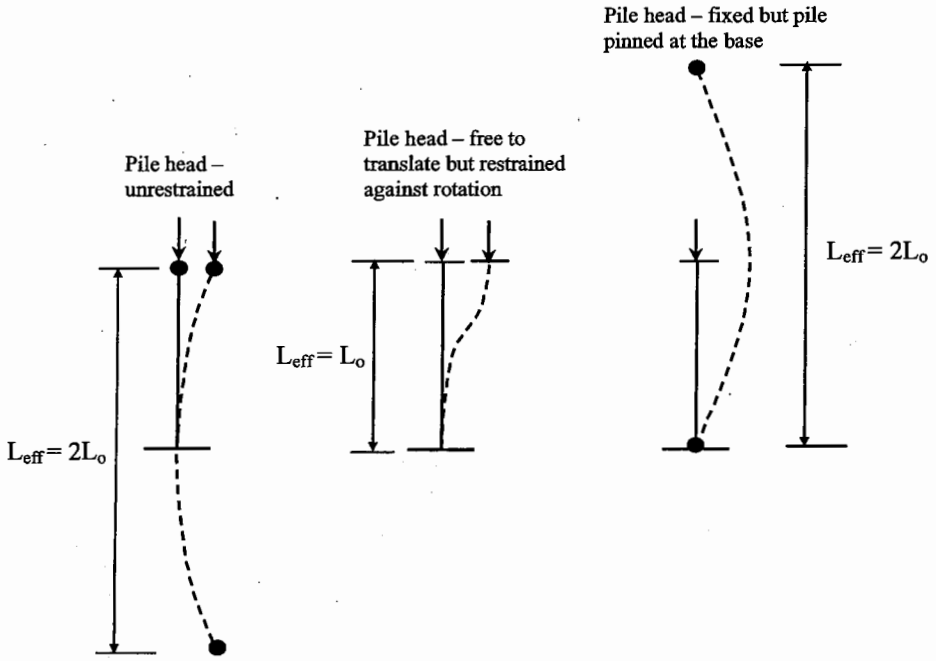

Fig. 3(a). Concept of effective length, adopted from Bhattacharya et al. (2004)

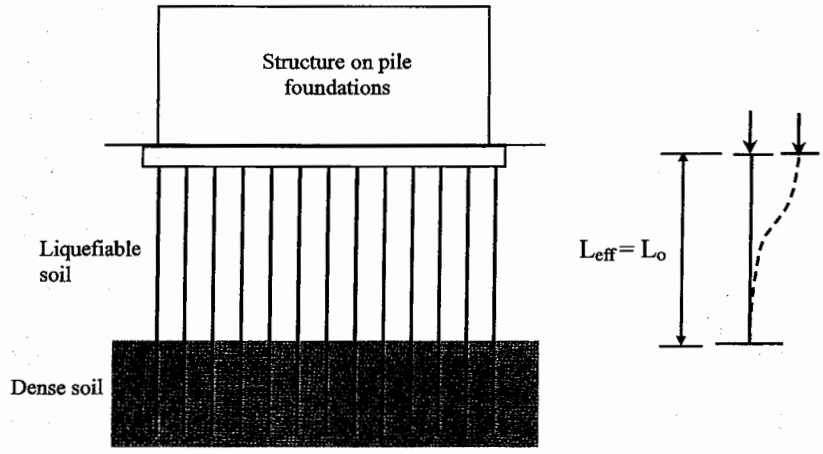

Fig. 3(b). Effective length of pile in case of a large raft supported on piles

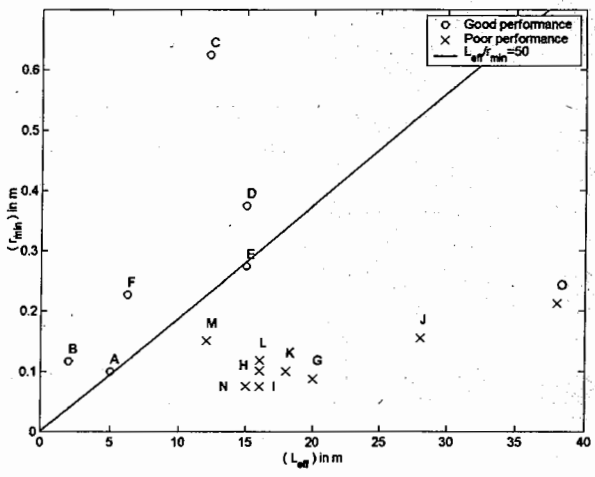

Fig. 4. L_{eff} versus r_{min} for piles studied, Bhattacharya et al. (2004)

assumed unsupported length) greater than 70. This is exactly the regime in which plastic buckling was predicted under a combination of axial and lateral load, corresponding in Fig. 2 to the 0.6 m pile being unsupported over a cantilever length of greater than 7 m. On the other hand, the analysis of the case histories shows that piles with a (P/P_E) ratio below 0.1 and a slenderness ratio smaller than 50 survived earthquakes even though they carried loads through soils that were spreading laterally.

The evidence of field studies in Figs. 4 and 5 is therefore consistent with the hypothesis that pile failure in liquefied soils is similar to the plastic buckling of structural columns in air. The lateral support offered to the pile by the soil prior to an earthquake seems capable of being removed during liquefaction. It may therefore not be relevant to invoke lateral spreading of the soil as the *cause* of pile collapse since piles can collapse by plastic

buckling as soon as sufficient soil has liquefied, and before lateral spreading takes place. Nevertheless, doubt may still be expressed on account of the assumption that the pile axial loads in the case histories could be approximated by the permissible axial loads. Laboratory tests under controlled conditions were used to dispel this final uncertainty.

PILE BUCKLING IN A CENTRIFUGE TEST

Dynamic centrifuge tests were carried out at Cambridge to verify that fully embedded piles, passing through saturated, loose to medium dense sands, and end-bearing on hard layers, buckle under the action of axial load alone if the surrounding soil liquefies in an earthquake. During earthquakes, whether at model or field scale, the axial loads on a pile are accompanied by lateral loads induced by the inertia of the superstructure and the drag of laterally spreading soil. The failure of a pile can arise because of any one of these load effects, or a suitable combination of them. The centrifuge tests were designed in level ground to avoid the effects of lateral spreading. Twelve piles were tested in a series of four centrifuge tests including some which decoupled the effects of inertia and axial load. The model piles were made of dural alloy tube having an outside diameter of 9.3 mm, a thickness of 0.4 mm and a total length of 160 mm or 180 mm. Properties of the model pile can be seen in Bhattacharya et al. (2004). The sand used to build the models was Fraction E silica sand, which is quite angular with D_{50} grain size of 0.14 mm, maximum and minimum void ratio of 1.014 and 0.613 respectively, and a specific gravity of 2.65. Axial load (P) was applied to

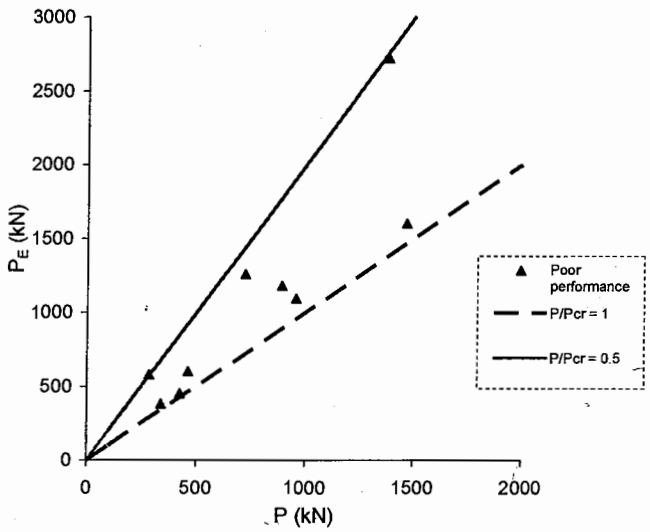

Fig. 5. Plot of P and P_E of the poor performance piles in Table 1

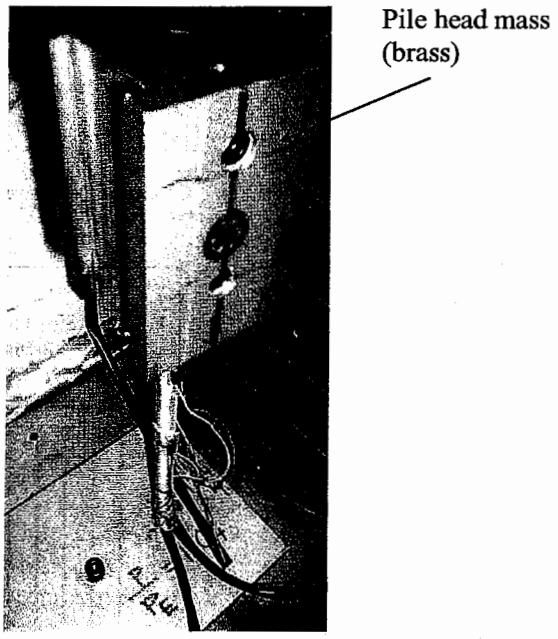

Fig. 6. Loading arrangement for pile 10

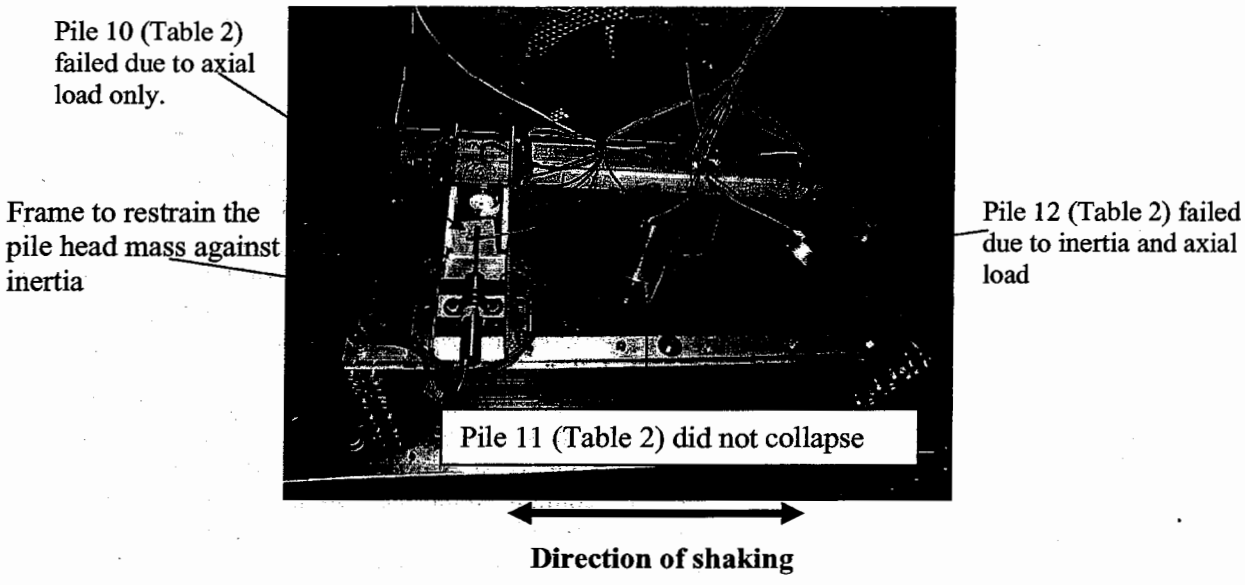

Fig. 7. Surface observations after the test SB-06

Table 2. Summary of the centrifuge tests

Test ID	Pile ID	Max load (P) N	$\sigma = P/A$ MPa	P/P_E	Load effects	Remarks	Reference
SB-02 Pile length = 160 mm Area (A) = 9.7 mm^2 RD = 48%	1	768	79	0.97	Axial + Inertia	Failed	For details of tests SB-02, SB-03 and SB-04 *see* Bhattacharya et al. (2004) Bhattacharya (2003).
	2	642	65	1.01	Axial + Inertia	Failed	
	3	617	63	0.97	Axial + Inertia	Failed	
SB-03 Pile length = 180 mm Area (A) = 11.2 mm^2 RD = 45%	4	294	26.3	0.5	Axial + Inertia	Did not fail	
	5	220	19.7	0.35	Axial + Inertia	Did not fail	
	6	113	10.1	0.22	Axial + Inertia	Did not fail	
SB-04 Pile length = 180 mm Area (A) = 11.2 mm^2 RD = 43%	7	610	54.5	1.04	Axial	Failed	
	8	872	78	1.48	Axial	Failed	
	9	2249	201	0.25	Axial	Did not fail	
SB-06 Pile length = 180 mm Area (A) = 11.2 mm^2 RD = 40%	10	735	65.6	1.25	Axial	Failed	This paper describes the results of Pile 10.
	11	269	24	0.46	Axial + Inertia	Did not fail	
	12	441	39.4	0.75	Axial + Inertia	Failed	

σ = axial stress in the pile, RD = Relative density of the soil.

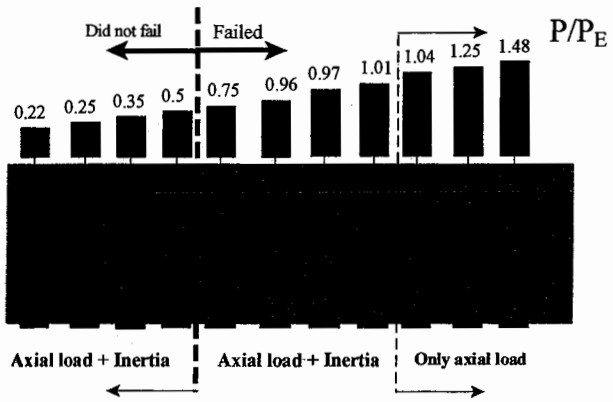

Fig. 8. Schematic representation of the test results

the pile through a block of brass fixed at the pile head (Fig. 6). With the increase in centrifugal acceleration, the brass weight imposes increasing axial load in the pile.

The packages were centrifuged to 50 g, one-dimensional earthquakes were fired and the soil liquefied. The effect of axial load alone was studied by using a specially designed frame (shown post-earthquake in Fig. 7) to restrain the head mass against inertial action, leaving it free to move orthogonal to the direction of shaking. Table 2 and Fig. 8 summarise the performance of the piles along with the load effects acting. Emphasis is given to the normalised axial load (P/P_E) where P is applied axial load or the axial load at failure. The piles marked 7 and 8 in test SB-04 were tested in similar conditions (in test SB-05 not included in Table 2) but in the absence of soil, thereby simulating classical Euler buckling. Thus, through the series of tests, the various influences on pile behaviour could be distinguished. Details of the early tests can be found in Bhattacharya et al. (2004), while this paper details test SB-06 which was aimed at revealing the exact sequence of events leading to pile failure.

As can be seen from Table 2 and Fig. 8, axial loads applied to the piles ranged from 22% to 148% of Euler's elastic critical load (P_E) treating piles as long columns and neglecting any support from the soil. Only those piles having P/P_E ratio greater than 0.75 failed. This is consistent with the case histories where the piles that failed had a (P/P_E) ratio between 0.5 and 1 (*see* Fig. 5). The loads in the piles marked 7, 8 and 10 (*see* Table 2) were purely axial. The pile heads were restrained in the direction of shaking (no inertia effects) and the piles buckled transversely to the direction of shaking. It must also be remembered that the piles were carrying the same load (load at which it failed) at 50 g and was stable before the earthquake. The axial stress in the pile sections was well within the elastic range of the material (less than 30% of the yield strength) but they failed as the earthquake was fired. This further supports the hypothesis that pile buckling is initiated when soil liquefies. It should be noted that $P/P_E = 0.75$, $P/P_Y = 0.25$ gives $P/P_R = 1$ according to Eq. (2), a combination that conforms very well to Rankine's criterion of plastic buckling.

This paper presents new detailed results for pile 10 in Table 2 which leave the matter in no doubt. Figure 9 shows the instrumentation layout surrounding the pile with an estimate of the pre-existing effective vertical stress (σ'_v) at the corresponding elevation. A spring-loaded LVDT was held against the pile head to follow the movement of the pile head. Near field pore pressures were also measured by placing the PPT's very close to the pile. Miniature Entran earth pressure cells SC2 and SC3 were attached to the front and back faces of the pile at 75 mm depth (representing 3.75 m depth of soil in the prototype scale) to record the total pressure changes as the pile buckles. Figure 7 showed the surface observation after test SB-06 and Fig. 10 reveals the mode shape of pile 10 during excavation following that test. It may be observed that the pile head rotated, which is quite similar to the

observation of piled buildings in the aftermath of a real earthquake, and again conforms with the plastic buckling hypothesis.

Figure 11 plots the time histories of input acceleration, pore pressure records and the LVDT readings. It may be noted that from the PPT records that as shaking starts (0.22 s in the time history) pore pressures begin to rise. The LVDT record on the other hand shows that the pile starts to move unidirectionally at around 0.26 s in the time history i.e. after two full cycles of loading. It must also be remembered that this unidirectional movement is orthogonal to the direction of shaking and thus denotes the onset of buckling instability. This confirms that the plastic buckling is not linked to inertia loads in this test. It must also be noted that the pile begins to buckle before the bottom soil (PPT 6266 in Fig. 9) achieves full liquefaction ($r_u = 82\%$).

It has been observed through the analysis of pore pressure data in centrifuge tests, Bhattacharya et al. (2003), that as shaking starts the pore pressure rises such that the condition of zero effective stress is achieved first at the soil top surface, advancing swiftly downwards as a liquefaction front. It is hypothesised that, with the advancement of this front, the pile will progressively loose the lateral bracing of the surrounding grains. When

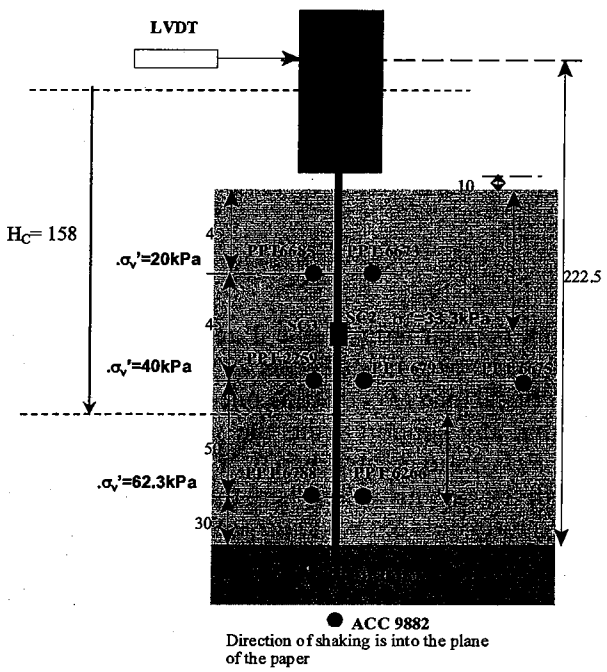

Fig. 9. Instrumentation layout surrounding pile 10 (all dimensions is in mm)

Fig. 10. Mode shape of pile 10 after the test during excavation

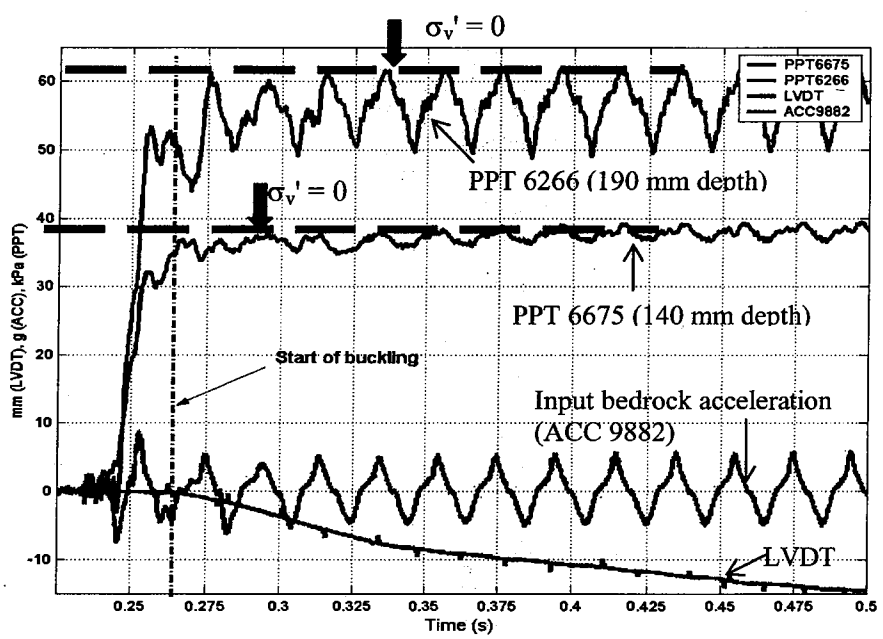

Fig. 11. Time histories of input acceleration, pore pressure and LVDT reading for pile 10

this advancing front reaches a critical depth H_c, Eq. (4) together with the condition $L_{eff}=2H_c$ for a pile with no restraint at the head (Fig. 3) gives:

$$H_c=\sqrt{\frac{\pi^2 EI}{4P}} \quad (5)$$

For pile 10, the critical depth (H_c) is thereby calculated to be 158 mm from the point of application of the axial load, taken as the centre of the brass weight. This suggests a point of fixity 18 mm below the level at which PPT 6675 was placed. Figure 11 shows that PPT 6675 indicated full liquefaction, whereas PPT 6266, which is 32 mm below the theoretical depth H_C, had not fully liquefied when the pile started to buckle. Equation (5) is therefore well-supported by the experimental evidence. It might be thought to be surprising that the undrained shear strength of the initially liquefied sand was incapable of supplying sufficient resistance to prevent buckling. It is well known that even relatively loose sands indulge in suppressed dilation, with consequential pore pressure reduction and effective stress increase, when sheared monotonically and with limited drainage. Takahashi et al. (2002) studied the lateral resistance of model piles pushed laterally through a liquefied soil. The displacement rate of the cylinder was varied from 1 mm/s to 100 mm/s, using pore fluids of different permeabilities. Their test results showed that the initial resistance to movement is negligible at all rates of loading but that some resistance was mobilised after a certain amount of displacement. They further concluded that higher the rate of loading the larger is the resistance. Towhata et al. (1999) reached similar conclusions. Further evidence of ultimate lateral resistance can be derived from the data of the earth pressure cells used with pile 10 in test SB-06.

The difference in the readings of the stress cells (SC2 and SC3 in Fig. 9) can be taken to indicate the lateral resistance offered by the liquefied soil to the buckling pile. This lateral resistance can be normalised by the initial effective over burden pressure (33.3 kPa) at the level of the pressure cells. The pile displacement (δ) at the level of the earth pressure cells (i.e. at 75 mm depth) can be estimated from the LVDT record of pile head displacement using an interpolation based on a parabolic mode shape. Figure 12 shows the plot of normalised lateral resistance against the normalised lateral displacement of the pile (δ/D) which can be regarded a local reference strain. It may be noted that lateral resistance increases drastically after 30% reference strain. This explains why the rate of failure reduces after 0.325 s, as seen in the LVDT record of Fig. 11. The liquefied soil then offers some resistance, but it cannot prevent the evolution of plastic buckling since the pile head had by then displaced by about one pile diameter, and the instability was unstoppable. One consequence of the large-strain resistance is taken to be the location of the ultimate plastic hinge, well above the base of the zone that initially liquefied.

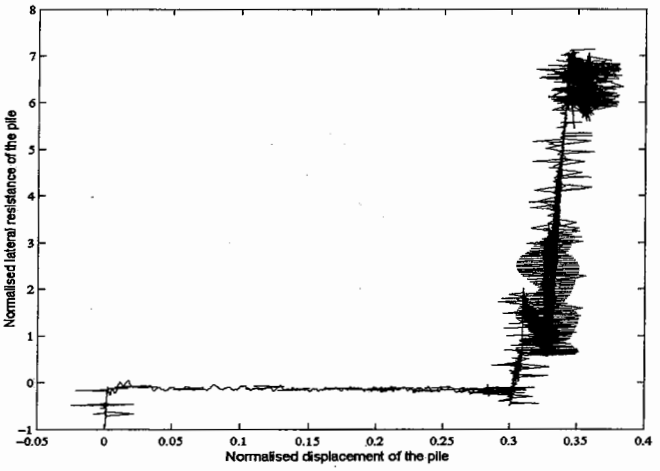

Fig. 12. Normalised lateral resistance versus normalised lateral displacement (δ/D)

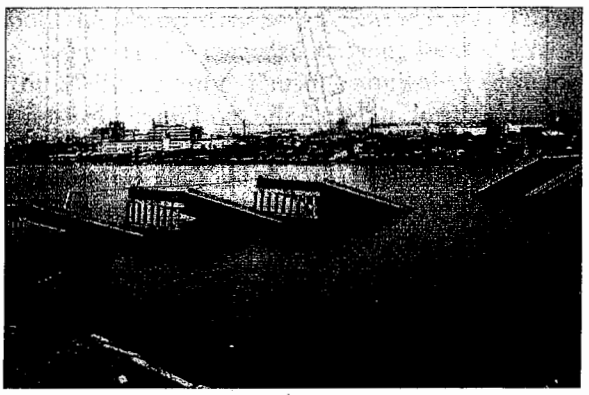

Fig. 13. Failure of Showa Bridge

FAILURE OF THE SHOWA BRIDGE DURING THE 1964 NIIGATA EARTHQUAKE

This section describes the Showa Bridge and the damage due to the 1964 Niigata earthquake, as a proposed example of pile failure by buckling. It will be shown that the piles satisfy the calculation criteria of the JRA (1996) code section 7.3, i.e. have enough apparent strength to resist lateral spreading, but they failed. This will be explained as being a consequence of axial loads.

The bridge was built over the Shinano river and was completed just a month before the earthquake (Fukoka, 1966). The bridge had a width of 24 m and total length of 303.9 m. The superstructure of the bridge consisted of 12 composite girders. The foundations of each pier consisted of a single row of 9 tubular steel piles connected laterally as shown in Fig. 13. After the earthquake five girders (G_3 to G_7) fell into the river as shown in Fig. 14. Figure 15 shows the post earthquake failure investigation and recovery of a damaged pile, together with the soil investigation data. Table 3 summarises the design data of the pile.

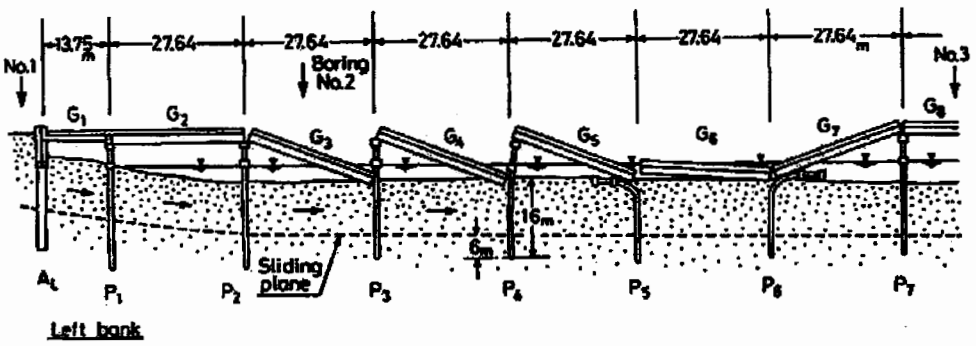

Fig. 14. Schematic diagram of the fall-off of the girders in Showa Bridge (Takata et al., 1965)

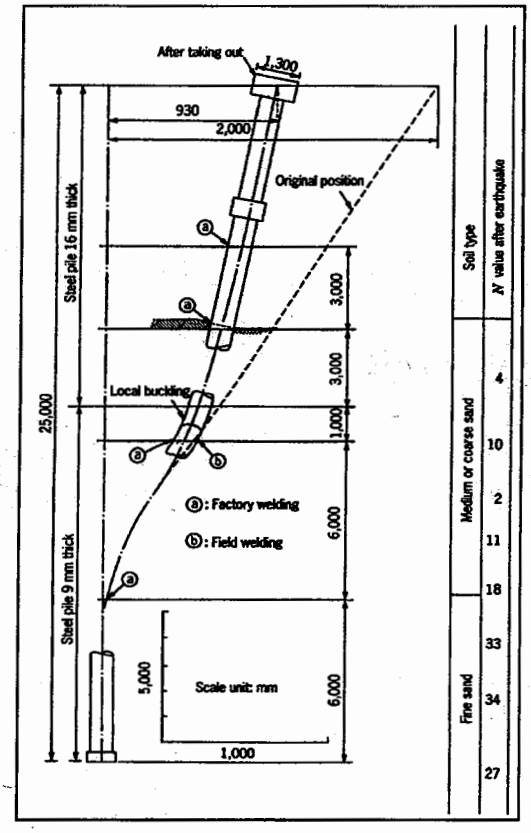

Fig. 15. Failed pile and the soil profile, Fukoka (1966)

Table 3. Design data of pile

Length	25 m
External diameter	609 mm
Internal diameter	591 mm
Material	Steel
E (Young's modulus)	210 GPa

Eyewitness Report

According to a reliable eyewitnesses, "the girders began to fall somewhat later, perhaps about 0 to 1 minute after the earthquake motion ceased", Hamada (1992a). As can be seen from Fig. 14, the piles of pier P_5 displaced towards the left and the piles of pier P_6 displaced towards the right (Fukoka, 1966). Had the cause of pile failure been due to lateral spreading, as suggested by Hamada (1992a) the piers should have displaced identically in the direction of the slope. Furthermore, the piers close to the riverbanks did not fail, whereas here the lateral spread was seen to be severe.

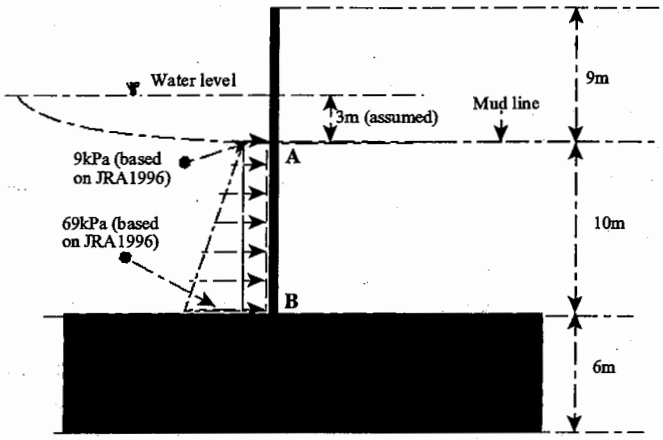

Fig. 16. Schematic diagram showing the predicted loading based on JRA code

Bending Calculation Based on JRA (1996) Code

Figures 13 and 14 indicate that the soil surrounding the failed piles was a fully submerged sand, so it would be unwarranted to invoke a non-liquefied crust in this case. Figure 16 shows the design lateral loading diagram based on section 7.3 of the JRA (1996) code. The calculation below estimates the maximum bending moment *ignoring axial load effects*.

Assume the bulk unit weight of soil is 20 kN/m^3.

Maximum lateral spreading pressure at mudline at point A in Fig. 16 = 30% of total overburden pressure due to water = 0.3×10 kN/m$^3 \times 3$ m = 9 kPa.

Maximum lateral spreading pressure at 10 m depth acting at point B in Fig. 16 = 30% of total overburden pressure = $0.3 \times (20$ kN/m$^3 \times 10$ m + 10 kN/m$^3 \times 3$ m) = 69 kPa.

Maximum bending moment, at point B in Fig. 20, due to spreading forces (trapezoidal loading)

= (0.5 × 60 kPa × 10 m × 0.609 m × 3.33 m) + (9 kPa ×

10 m × 0.609 m × 5 m)
= 608 kNm + 274 kNm = 882 kNm.
The plastic moment capacity of the section AB (9 mm thick)

$$= \left(\frac{0.609^3}{6} - \frac{0.591^3}{6} \right) \text{m}^3 \times 500 \text{ MPa} = 1620 \text{ kNm}$$

Hence the calculated factor of safety against plastic bending failure, ignoring axial load effects, is (1620/882) = 1.84.

Thus, according to this provision of JRA code i.e. section 7.3 of JRA (1996), the bridge should not have collapsed. Following the 1964 collapse, a law was passed to prevent bridge piers being founded on a single row of piles. The structural mechanics which explains the collapse will now be explained.

Buckling Calculations

For the Showa Bridge piles, the estimated allowable load is 965 kN and the theoretical buckling load (assuming liquefied soil did not offer support) is 1030 kN i.e. only 7% greater. The calculations are given below.

Axial Load at Failure

The dead load on each pile can be deduced from the configuration of the Showa Bridge deck. Information on the dimensions of the girders, span and the bridge type is obtained from Iwasaki (1984). Reasonable assumptions are made for the missing data. A schematic diagram of the deck is shown in Fig. 17. The bridge has a total length of 303.9 m (13.75 m + 10@ 27.64 m + 13.75 m) and width of 24 m. As mentioned earlier, the superstructure of the bridge consists of 12 composite steel simple span girders. There are 9 piles in a row sharing the load of the superstructure (*see* Fig. 13). Table 4 shows the estimate of the total dead load for each span. It is assumed in the analysis that the load of the deck is shared equally by the 9 piles. The dead load per pile is approximately 740 kN. If the live load due to vehicles were added, the total axial load P at the time of failure would be roughly 800 kN. An allowable vertical load calculated on the basis of soil resistance (SPT N values) was found to be 965 kN, Bhattacharya (2003), which is entirely reasonable viewed in isolation.

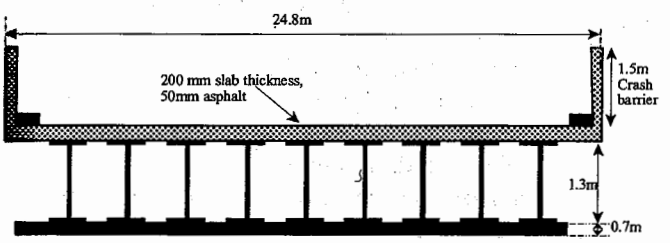

Fig. 17. Schematic of the Showa Bridge deck (adapted from Iwasaki, 1984)

Elastic Critical Load

The length of the pile in the liquefiable soil zone is about 9 m according to Fig. 15, but the underlying denser sand can be estimated to require a further 2 m of embedment to provide moment fixity in the event of liquefaction. The additional length of the structural column extending the pile and passing through water and air to support the bridge deck is 9 m. In addition, the bridge dead weight can be regarded as being located 1 m above the top of the column. Thus the equivalent unsupported length of the cantilever pile/column during liquefaction is $L_o \approx 21$ m. From the buckled shape (shown as the original position in Fig. 15), it is clear that the pile had a fixed-free boundary condition in the fashion of Fig. 3(a), and hence the effective buckling length $L_{\text{eff}} = 2L_o \approx 42$ m. It should perhaps be mentioned that the elastic stiffness of the pile has ignored any contribution from the soil inside, as is conventional in foundation engineering.

The lower pile section, as detailed in Fig. 15, is the 0.6 m diameter 9 mm thick steel tube that was chosen for the worked example leading to Fig. 2. It may be seen from there that an 800 kN axial load should ideally buckle elastically at $L_o \approx 22$ m, but that Rankine's estimate of the unsupported plastic buckling length is $L_o \approx 21$ m. There is an apparently perfect match with the earlier estimate of the unsupported length assuming that the loose sand liquefied. However, a small correction should be made.

Whereas the lower 8 m of the unsupported length is a 9 mm thick tube, the upper 13 m is a 16 mm tube with a welded connection about 3 m below the river bed as shown in Fig. 15. Timoshenko and Gere (1961) article

Table 4. Dead load calculation for Showa Bridge

Item	Details	Load
Slab and asphalt top	24.8 m × 27.64 m × (0.2 + 0.05) m × 25 kN/m^3	4146 kN
Crash barrier	2 × 1.5 m × 0.1 m × 27.64 × 25 kN/m^3	207.3 kN
Kerb	2 m × 0.15 m × 27.64 m × 25 kN/m^3	207 kN
9 steel girders	27.64 m × 9 × 5.2 kN/m	1294 kN
Stiffeners, bolts	30% of girder weight	388 kN
Bottom girder	0.7 m × 1.0 m × 24 m × 25 kN/m^3	420 kN
Total		6662 kN
Load per pile = 6662 kN/9		740 kN

2.14 provide an analytical solution for a column of varying section. The solution proceeds in terms of an upper length L_1 with bending stiffness EI_1 and a lower length L_2 with bending stiffness EI_2. Corresponding buckling parameters k_1 and k_2 are defined such that $k_1^2 = P_E/EI_1$, $k_2^2 = P_E/EI_2$, where P_E is the axial load in both sections at the elastic critical load (recalling that there is no skin friction to be applied in liquefied soil). The solution is found in the form of the transcendental equation:

$$\tan k_1 L_1 \tan k_2 L_2 = k_1/k_2 \qquad (6)$$

On substituting $L_1 = 13$ m, $EI_1 = 275$ MNm^2, $L_2 = 8$ m, $EI_2 = 160$ MNm^2, a solution is found by iteration for which $k_1 = 0.0612$ m^{-1} and $k_2 = 0.0803$ m^{-1} at $P_E = 1030$ kN. The comparative buckling load if the lower section applied throughout, given an effective buckling length $L_{eff} = 21 \times 2 = 42$ m, would have been 895 kN as shown below.

Moment of inertia of the pile (I) =

$$\frac{\pi}{64}(0.609^4 - 0.591^4)\text{m}^4 = 7.63 \times 10^{-4}\text{m}^4$$

Effective length of pile (L_{eff}) = 2×21 m = 42 m

Buckling load of pile (P_E) = $\dfrac{\pi^2}{L_{eff}^2} EI$

$$= \frac{\pi^2}{42^2\text{m}^2} \times 210\ \text{GPa} \times 7.63 \times 10^{-4}\text{m}^4 = 895\ \text{kN}$$

The factor 1.72 enhancement of stiffness in the upper section has resulted only in a factor 1.15 on the elastic buckling load, since it is the lower, lighter section that has the greater curvature in the cantilever buckling mode. Thus the buckling load of the pile $P_E = 895 \times 1.15 = 1030$ kN.

The 15% increase in the theoretical elastic buckling load due to stiffening can equally be applied as a reduction factor to the previously estimated axial load so that Fig. 2 can still be used to discuss unsupported lengths in relation to buckling failures. The equivalent axial load is then 800/1.15 kN = 696 kN. Figure 2 then shows that a purely elastic column, under axial load alone, would buckle if its unsupported length were 24 m. Accepting Rankine's estimate of the plastic buckling load, failure would occur for an unsupported length of 23 m. Since the estimated unsupported length is 21 m, immediate failure is not now indicated under axial load alone. However, it is also clear that the back-analysis puts the state point of the Showa Bridge piles deeply into the impermissible region with $P/P_E = 800/1030 = 0.78$, whereas $P/P_E < 0.33$ is considered advisable if lateral loads are also involved.

It is interesting to speculate on whether the marginal factor of safety against plastic buckling, represented by the difference in unsupported length between the presumed 21 m and the 23 m calculated at failure, explains the delay of up to a minute between the earthquake and the collapse of the bridge. It may be that excess pore pressures created in the liquefiable sand zone propagated downwards to cause softening in the zone of pile support. Or it may be that inertia induced in the bridge deck during the earthquake created sufficient lateral load on the pile cap to ratchet the structure into instability after liquefaction. The magnification factor on lateral load effects with $P/P_E = 0.78$, according to Eq. (1), is 4.5, so every unit of lateral load actually induced during liquefaction-buckling would have had 4.5 times the severity of a lateral load applied in the absence of axial load. The crucial aspect raised in the foregoing analysis, to which no code of practice currently draws attention, is the overwhelming importance of the axial loads on the piles in relation to their buckling loads, considering their likely unsupported lengths following soil liquefaction.

CONCLUSIONS

1. Case studies of the performance of piled foundations in earthquakes, and centrifuge tests on slender model piles not subject to lateral spreading or inertia effects, have proved that buckling is a possible failure mechanism for piled foundations subject to seismic liquefaction. Euler's elastic buckling load P_E should be calculated on the basis of an effective length L_{eff} deduced from the unsupported length L_o that allows for liquefaction and for the needs of pile fixity in underlying non-liquefied ground. Structural fixity should be taken into account. The squash load P_P at plastic yielding should also be calculated, so that Rankine's plastic buckling load P_R can be estimated using Eq. (2).
2. If axial loads exceed P_R piles will buckle in the event of seismic liquefaction even if there are no lateral loads acting at the same time. Lateral load effects due to soil drag accompanying slope movement, or to inertia loads accompanying pre-liquefaction shaking, should first be calculated in the absence of axial loads effects, and then magnified using Eq. (1) accounting for axial loads. If the magnified bending moment exceeds the plastic capacity of the pile in the unsupported zone, the pile will fail by plastic buckling and bending. A back-analysis of the failure of the Showa Bridge in the Niigata earthquake of 1964 suggests that axial loads would have amplified bending moments due to soil spreading or to structural inertia by a factor as high as 4.5. It is proposed that this caused the collapse.
3. These considerations suggest that piles in liquefiable soils should enjoy a factor of safety of at least 3 against Euler's elastic buckling. In contrast, all current codes of practice for pile design omit considerations necessary to avoid buckling in event of soil liquefaction. This oversight could be acceptable only if piles in liquefiable soil were designed to have a slenderness ratio smaller than 50, so that buckling is sufficiently remote. The temptation to use groups of easily driveable slender piles of great depth, which could be a feasible and economic foundation solution in other

circumstances, should be avoided if surrounding soils can liquefy in earthquakes.

4. Initially liquefied soil cannot prevent the initiation of buckling, but suppressed dilation can offer some large-displacement lateral resistance which can dictate the ultimate location of a plastic hinge.
5. Future research, development and statutory regulation for piled foundations should focus on:
   - Further elaboration of the overall structural response of pile groups carrying axial loads through spreading, liquefied soils with a view to refining design load combinations.
   - Retrofitting measures for existing piled foundations found to be subject to buckling.
   - Promulgation of new rules to forbid unprotected slender piles and encourage the use of fewer, high modulus piles and cellular arrangements.

REFERENCES

1) Abdoun, T. and Dobry, R. (2002): Evaluation of pile foundation response to lateral spreading, *Soil Dynamics and Earthquake Engineering*, 22, 1051–1058.
2) Berrill, J. B., Christensen, S. A., Keenan, R. P., Okada, W. and Pettinga, J. R. (2001): Case studies of lateral spreading forces on a piled foundation, *Geotechnique*, **51** (6), 501–517.
3) Bhattacharya, S. (2003): Pile instability during earthquake liquefaction, *PhD Thesis*, University of Cambridge (U.K).
4) Bhattacharya, S., Madabhushi, S. P. G. and Bolton, M. D (2003): Pile instability during earthquake liquefaction, *Proc. 16th ASCE Engrg. Mech. Conf. (EM-03)*, Paper No. 404, University of Washington, Seattle, 16–18th July, Also available at www.ce.washington.edu/em03/proceedings/papers/404.pdf
5) Bhattacharya, S., Madabhushi, S. P. G. and Bolton, M. D. (2004): An alternative mechanism of pile failure in liquefiable deposits during earthquakes, *Geotechnique*, **54** (3), 203–213.
6) Eurocode 8 Part 5 (1998): Design provisions for earthquake resistance of structures-foundations, retaining structures and geotechnical aspects, *European Committee for Standardization*, Brussels.
7) Finn, W. D. L. and Fujita, N. (2002): Piles in liquefiable soils: seismic analysis and design issues, *Soil Dynamics and Earthquake Engineering*, 22, 731–742.
8) Finn, L. W. D. and Thavaraj, T. (2001): Deep foundations in liquefiable soils: Case histories, centrifuge tests and methods of analysis, *Proc 4th Int. Conf. Recent Advances in Geotechnical Earthquake Engineering and Soil Dynamics*, 26–31, March San Diego, California.
9) Fleming, W. G. K., Weltman, A. J., Randolph, M. F. and Elson, W. K. (1992): *Piling Engineering*, 2nd ed., John Wiley & Sons.
10) Fukoka, M. (1966): Damage to civil engineering structures, *Soils and Foundations*, **6** (2), 45–52.
11) Goh, S. and Rourke, T. D. (1999): Limit state model for soil-pile interaction during lateral spread, *Proc. 7th. U.S.-Japan Workshop on Earthquake Resistant Design of Lifeline Facilities and Countermeasures against Soil Liquefaction, Seattle, WA.*
12) Haigh, S. K. and Madabhushi, S. P. G. (2002): Centrifuge modelling of lateral spreading past pile foundations, *Proc. Int. Conf. Physical Modelling in Geotechnics*, St. John's Newfoundland, Swets & Zeitlinger Lisse, 471–475.
13) Hamada, M. (1992a): Large ground deformations and their effects on lifelines: 1964 Niigata earthquake, *Case Studies of Liquefaction and Lifelines Performance during Past Earthquake, Technical Report NCEER-92-0001, Volume-1, Japanese Case Studies, National Centre for Earthquake Engineering Research*, Buffalo, NY.
14) Hamada, M. (1992b): Large ground deformations and their effects on lifelines: 1983 Nihonkai-Chubu earthquake, *Case Studies of Liquefaction and Lifelines Performance during Past Earthquake, Technical Report NCEER-92-0001, Volume-1, Japanese Case Studies, National Centre for Earthquake Engineering Research*, Buffalo, NY.
15) Hamada, M. (2000): Performances of foundations against liquefaction-induced permanent ground displacements, Paper 1754, *Proc. 12th World Conf. Earthquake Engineering*, Auckland, New Zealand.
16) Hetenyi, M. (1946): *Beams on Elastic Foundations*, The University of Michigan Press.
17) Horne, M. R. and Merchant, W. (1965): *The Stability of Frames*, Pergamon.
18) IS-1893 (2002): Criteria for earthquake resistant design, Bureau of Indian Standard (BIS), New Delhi, India.
19) Ishihara, K. (1993): Liquefaction and flow failure during earthquakes, *Geotechnique* **43** (3), 351–415.
20) Ishihara, K. (1997): Terzaghi oration: Geotechnical aspects of the 1995 Kobe earthquake, *Proc. ICSMFE*, Hamburg, 2047–2073.
21) JRA (1996): Japanese Road Association, *Specification for Highway Bridges, Part V, Seismic Design.*
22) National Earthquake Hazards Reduction Program (NEHRP) (2000): Commentary (Federal Emergency Management Agency, USA, 369) for seismic regulations for new buildings and other structures.
23) National Research Council (NRC) (1985): Liquefaction of soils during earthquakes, National Academic Press, Washington, DC.
24) Ramos, R., Abdoun, T. H. and Dobry, R. (2000): Effects of lateral stiffness of superstructure on bending moments of pile foundation due to liquefaction induced lateral spreading, *Proc. 12th World Conf. Earthquake Engineering*, Auckland, New Zealand.
25) Rankine, W. J. M. (1866): *Useful Rules and Tables*, London.
26) Sato, M., Ogasawara, M. and Tazoh, T. (2001): Reproduction of lateral ground displacements and lateral-flow earth pressures acting on pile foundations using centrifuge modelling, *Proc. 4th Int. Conf. Recent Advances in Geotechnical Earthquake Engineering and Soil Dynamics*, 26–31, March, San Diego, California.
27) Schofield, A. N. and Wroth, C. P. (1968): *Critical State Soil Mechanics*, McGraw-Hill, London.
28) Soga, K. (1997): Chapter 8, Geotechnical aspects of Kobe earthquake, *EEFIT Report*, Institution of Structural Engineers, UK.
29) Takahashi, A., Kuwano, Y. and Yano, A. (2002): Lateral resistance of buried cylinder in liquefied sand, *Proc. Int. Conf. Physical Modelling in Geotechnics, ICPMG-02*, 10–12 July, St. John's, Newfoundland, Canada.
30) Takata, T., Tada, Y., Toshida, I. and Kuribayashi, E. (1965): Damage to bridges in Niigata earthquake, *Report No. 125-5*, Public Works Research Institute (in Japanese).
31) Timoshenko, S. P. and Gere, J. M. (1961): *Theory of Elastic Stability*, McGraw-Hill Book Company, New York.
32) Tokimatsu, K, Mizuno, H. and Kakurai, M. (1996): Building damage associated with geotechnical problems, *Special Issue of Soils and Foundations*, 219–234.
33) Tokimatsu K., Oh-oka H., Satake, K., Shamoto, Y. and Asaka, Y. (1998): Effects of lateral ground movements on failure patterns of piles in the 1995 Hyogoken-Nambu earthquake, *Proc. A Speciality Conf., Geotechnical Earthquake Engineering and Soil Dynamics III, ASCE Geotechnical Special Publication*, **75**, 1175–1186.
34) Tokimatsu, K., Suzuki, H. and Suzuki, Y. (2001): Back-calculated *p-y* relation of liquefied soils from large shaking table tests, *Proc. 4th Int. Conf. Recent Advances in Geotechnical Earthquake Engineering and Soil Dynamics*, 26–31, March, San Diego, California.
35) Towhata, I., Vargas-Mongem, W., Orense, R. P. and Yao, M. (1999): Shaking table tests on subgrade reaction of pipe embedded in sandy liquefied subsoil, *Soil Dynamics and Earthquake Engineering*, **18** (5), 347–361.
36) Yokoyama, K., Tamura, K. and Matsuo, O. (1997): Design methods of bridge foundations against soil liquefaction and liquefaction-induced ground flow, *2nd Italy-Japan Workshop on Seismic Design and Retrofit of Bridges*, 27–28, Feb., Rome, Italy.